

Quasiclassical Trajectory Study of NO Vibrational Relaxation by Collisions with Atomic Oxygen

James W. Duff

Spectral Sciences, Inc., 99 S. Bedford St., Burlington, Massachusetts 01803

Ramesh D. Sharma

Optical Environment Division (GPOS), Geophysics Directorate, Phillips
Laboratory, 29 Randolph Rd., Hanscom AFB, Massachusetts 01831

Abstract. Room temperature and temperature-dependent thermal rate constants are calculated for the state-to-state vibrational relaxation of $\text{NO}(v' 9)$ by atomic oxygen using the quasiclassical trajectory method and limited *ab initio* information on the two lowest O+NO potential energy surfaces which are responsible for efficient vibrational relaxation. Comparisons of the theoretical results with the available experimental measurements indicate reasonable agreement for the deactivation of $\text{NO}(v=2,3)$ at 300 K and $\text{NO}(v=1)$ at 2700 K, although the calculated relaxation rate constant for $\text{NO}(v=1)$ at 300 K is approximately a factor of 2 below the measured value. The state-to-state relaxation rate coefficients involve the formation of long-lived collision complexes and indicate the importance of multiquantum vibrational relaxation consistent with statistical behavior in O+NO collisions. The present results, combined with recent measurements of vibrational relaxation for $\text{NO}(v=2,3)$, suggest that the current atmospheric models of NO cooling rates require higher atmospheric temperatures and/or an increase in the NO/O number densities.

1. Introduction

Fundamental vibration-rotation band emission ($\Delta v=1$) from nitric oxide near $5.3 \mu\text{m}$ has been long known to be an important cooling mechanism in the terrestrial thermosphere.^{1,2} Vibrationally excited nitric oxide $\text{NO}(v=1)$, mostly $v=1$, may be produced by the collisions of ground state nitric oxide $\text{NO}(v=0)$ with atomic oxygen. It may also be produced, with vibrational excitation up to $v=18$, by the reaction of metastable $\text{N}(^2\text{D})$ atoms with O_2 ,



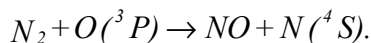
which is exothermic by 3.76 eV.³⁻⁵ This reaction may be the dominant process for the production of NO in the natural and artificial auroras. Highly rotationally and vibrationally excited NO may also be produced by the reaction of ground state $\text{N}(^4\text{S})$ atoms with O_2 ,



This reaction, although exothermic by 1.38 eV, has an energy barrier of 0.3 eV and therefore requires translationally hot $\text{N}(^4\text{S})$ atoms to proceed.⁶ Reaction (2) is an important source of NO in the quiescent day⁷ and night time^{8,9} thermosphere and may also be important in natural and artificial auroras. The fact this reaction requires translationally hot atoms to proceed may also explain the large variability of NO density with the geophysical parameters.¹⁰

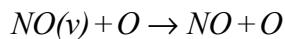
The reaction of N_2 with ground state $\text{O}(^3\text{P})$ atoms, known to be important in combustion where it produces highly vibrationally and rotationally excited NO,¹¹ may

also produce NO at very high altitudes in the terrestrial thermosphere where translationally hot O atoms abound,¹²



The vibration-rotation excitation of NO produced in the thermosphere by reaction (3), which is endothermic by 3.25 eV, would depend upon the excess energy available.

It is clear that vibrationally excited NO is abundant in the terrestrial thermosphere and the amount of cooling it can produce clearly depends not only upon the rate coefficient of collisional deexcitation of the vibrational level of the reactant NO but also on the vibrational level of the product NO. Vibrational relaxation of NO due to collisions with N₂ is much slower than due to collisions with O, therefore only collisions involving NO and O have been considered,



where the vibrational level of product NO has not been identified. The rate coefficient of Reaction (4) has been measured at room temperature by Fernando and Smith¹³ and by Lilenfeld,¹⁴ and for v=2 and 3 by Dodd et al.¹⁵ Surprisingly, the results of Dodd et al. for higher vibrational levels are small than those of earlier workers for v=1 by a factor of about 2.5. Glanzer and Troe,¹⁶ in their shock tube experiment at an effective temperature of 2700 K, however measure about the same rate coefficients for v=1 and 2. A calculation by Quack and Troe¹⁷ at 2100 K using a statistical adiabatic model gives a lower rate coefficient than their shock tube measurement by a factor of about 3. However, these authors assume that vibrational relaxation occurs only on the attractive ground state NO₂ potential energy surface.¹⁸⁻²³

Recent electronic structure calculations²³ have shown that two surfaces should be considered in NO vibrational relaxation by O. Thus, the previous calculations of Quack and Troe should be considered an underestimate.

The factor of 2.5 difference between the $v=1$ and $v=2$ rate coefficients, however, are important in atmospheric modeling because they correspondingly impact the NO and/or O densities. Furthermore, for the state-to-state vibrational relaxation of NO, there is only a single experimental measurement²⁴ for $v=3^*v_B=2$ and one theoretical study for $v=1^*v_B=0$ and $v=2^*v_B=0,1$.¹⁷ Given the importance of these questions and inconsistencies concerning NO relaxation to the atmospheric community, this work employs a quasiclassical trajectory study to obtain these rate coefficients as a function of the initial and final vibrational state of NO as a function of temperature.

2. Potential Energy Surfaces

Although the spectroscopy of the ground and excited states of the NO₂ molecule has received extensive theoretical attention over the last several decades,¹⁸⁻²² the potential energy surfaces of O(³P)+NO(X²Π) important for vibrational relaxation of NO are less well characterized. The only *ab initio* study of the interaction of O(³P)+NO(X²Π) is the recent work of Katagiri and Kato,²³ who obtained the asymptotic interaction of the 12 potential energy surfaces (neglecting spin-orbit coupling) correlating with O(³P)+NO(X²Π). Including the effects of the spin-orbit interaction, 18 adiabatic doubly-degenerate electronic states are obtained. Only the two lowest states are attractive, while the remaining 16 states are repulsive. Since it is well known that repulsive potentials are characterized by extremely inefficient vibrational energy transfer, the present study employs the lowest two adiabatic surfaces of ¹2AB and ¹2AC symmetry. A lack of any details concerning the

interactions among these surfaces precludes any dynamical investigation of nonadiabatic effects.

In addition to extensive studies on the bound NO_2 molecule, there has been considerable work on the *ab initio* $^2\text{ABPES}^{25,26}$ appropriate for $\text{N}+\text{O}_2$, Reaction (2), as well as several calculations of the reactivity using classical dynamics.^{6,25} However, the *ab initio* calculations have focussed on molecular geometries in the $\text{NO}+\text{O}$ product channel important for Reaction (2). The relationship of the $\text{NO}+\text{O}$ product channel from $\text{N}+\text{O}_2$ to the NO_2 molecule (and thus $\text{O}+\text{NO}$ relaxation) is extensively discussed by Gilibert et al.²⁵ where they have constructed correlation diagrams for several molecular geometries. Suzzi Valli et al.²⁶ have provided the most detailed calculations of the $\text{NO}+\text{O}$ product channel, however, again emphasizing molecular geometries most appropriate to the $\text{N}+\text{O}_2$ reaction. From these studies, it appears that a barrier of at least 2 eV exists between the $\text{N}+\text{O}_2$ reactants and the NO_2 molecule. Any evaluation of the current semiempirical $^2\text{ABPES}$ will have to await more extensive *ab initio* calculations at geometries relevant to Reaction (4).

The analytical form for the $\text{O}+\text{NO}$ PES is obtained by adding a term to describe the potential wells of the 1^2AB and 1^2AC surfaces to a London-Eyring-Polanyi-Sato (LEPS)²⁷ surface (which is taken to be the same for both electronic surfaces),

$$V(r_1, r_2, r_3) = V_{LEPS}(r_1, r_2, r_3) + V_A(r_1, r_2)$$

where r_1 , r_2 , r_3 are the NO , NO , and O_2 internuclear distances, respectively. The angular dependence and long-range behavior of the potential well is represented by a simple angular-dependent exponential function

$$V_A(r_1, r_2) = A(\Theta) \exp[-\gamma\{(r_1 - r^o) + (r_2 - r^o)\}]$$

where r^o is the location of the potential well, γ determines the range of the potential well. The angular dependence is given by a 3rd order polynomial in the ONO bond angle Θ

$$A(\Theta) = \sum c_k \Theta^k.$$

The attractive and repulsive diatomic potentials used in the LEPS function are represented by a modified Rydberg potential²⁸ and the anti-Morse function²⁷

$$V_R(r) = -D_e \left[1 + a_1(r - r_e) + a_2(r - r_e)^2 + a_3(r - r_e)^3 \right] \exp\{-a_1(r - r_e)\} + D_e$$

$$V_{AM}(r) = -D_e \left[1 + \exp\{-\beta(r - r_e)\} \right]^2 + D_e$$

where D_e is the dissociation energy, r_e is the equilibrium internuclear distance, (a_1, a_2, a_3) are parameters fit to the RKR potential, and $\beta = a_1/l$. In addition to the diatomic parameters defined above, the LEPS surface requires the specification of the adjustable Sato parameter, z_i , for each diatomic. Once the LEPS surface is determined, the $\{c_k\}$ in Equation (7) are determined such that the angular dependence of the potential at the equilibrium geometry defined by Equations (5)-(9) reproduces the *ab initio* calculations of Hirsch and Buenker²⁰ for the 1^2AB state and Gillispie et al.¹⁸ for the 1^2AC state (which correlates with the 2B_2 state in the strong interaction region²³). The final parameters for the 1^2AB and 1^2AC potential

energy surfaces are given in Table 1 for the LEPS function and Table 2 for the angular-dependent exponential function representing the potential well.

Contour plots of the 1^2A and $1^2A'$ angular dependence of potential energy surfaces are shown in Figures 1 and 2, respectively, for the NO bond distance fixed at its equilibrium internuclear value. For a wide range of bond angles, the approach of the O atom to the N end of the NO molecule occurs with no barrier. For the 1^2A PES the formation of NO_2 is favored for a wide range of bond angles ($\Theta \geq 85^\circ$) for approach of the O atom to the NO molecule, while the angular approach for the $1^2A'$ surface is more restrictive ($145^\circ \geq \Theta \geq 85^\circ$). The location, depth, and angular dependence of the potential wells for the bound NO_2 molecule on both surfaces are in qualitative agreement with the available *ab initio* calculations. However, no attempt was made to fit the available spectroscopic data of the stable triatomic NO_2 molecule for either the ground state 1^2A or excited state $1^2A'$ (which correlates with the 2B_2 state). The long range interaction is in good agreement with the *ab initio* calculations of Katigiri and Kato²³ for both surfaces, although due to the lack of information it has been assumed that there is no angular dependence to the long range attractive potential (i.e., the parameter γ in Equation (6) is independent of bond angle).

3. Classical Trajectory Methodology

The quasiclassical trajectory (QCT) method²⁹ is used to compute the thermal reaction rate constants, and the translational energy dependence of the reaction cross sections and the final vibrational/rotational state distributions. The validity of classical mechanics for calculating reaction rate constants and product distributions has been discussed elsewhere.²⁹ The classical approach is expected to be reliable for calculating state-to-state relaxation and reaction rate constants for which the transition or reaction probability is large (strongly classically allowed). Calculations

are carried out separately for the 1^2A and $1^2A'$ adiabatic potential energy surfaces and then combined after multiplying the individual rate constants by the temperature dependent electronic degeneracy factors (i.e., the probability of a collision occurring on a particular surface)

$$f(T) = 2 \{ [5 + 3 \exp(-227.8/T) + \exp(-326.6/T)] [2 + 2 \exp(-177.1/T)] \}^{-1}.$$

A thorough discussion of the spin-orbit effects and reactivity in the similar $O(^3P) + OH(^2\Pi)$ system is given by Graff and Wagner.³⁰

Standard Monte Carlo techniques are used to compute the vibrational relaxation rate constants as a function of temperature for specified initial vibrational states, v , where the translational energy, E_T , and the initial rotational states, j , are chosen from Boltzmann distributions at the given temperature. Final $NO(v_B j_B)$ distributions are also calculated as a function of initial vibrational state. The effect of electronic angular momentum on the NO rotational state has been ignored, as the NO diatomic properties appropriate to the $NO(X^2\Pi_{1/2})$ ground state have been used. The final vibrational and rotational quantum numbers $(v_B j_B)$ are obtained from the correspondence rules $v_{B_i} = (v_B + 2)h$ and $j_{B_i} = (j_B + 2)h$, where v_{B_i} and j_{B_i} are the classical vibrational and rotational action variables. The final $(v_B j_B)$ distributions are then obtained using the standard histogram method.

The classical equations of motion are integrated using a variable step size predictor-corrector method.³¹ Although this numerical integration scheme has been shown to accurately integrate long-lived classical trajectories in various systems,³¹⁻³³ approximately 5% of the trajectories forming collision complexes did not satisfy time-reversal criterion even though total energy and angular momentum were conserved. However, a survey of these trajectories indicated that while the individual trajectories

were inaccurate, the properties of the ensemble of trajectories were insensitive to the accuracy of the numerical integration (i.e., the error parameters). Thus, any error in the distributions reported here reflect the statistical uncertainty of the calculation. A total of 38,000 (19,000 for each PES) trajectories, of which approximately 1/2 (1/4) formed collision complexes on the $^2\text{AB}(^2\text{AC})$ PES, were used in the current study.

4. Results

The room temperature O+NO(v) relaxation rate constants are compared with the available experimental measurements in Figure 3. While the calculated $v=1$ to $v_B=0$ rate constant using the two lowest (attractive) potential energy surfaces is approximately a factor of 2 below the experimental measurements of Fernando and Smith¹³ and Lilenfeld,¹⁴ the QCT deactivation rate constants for $v=2$ and 3 are 30-40% greater than the measurements of Dodd et al.¹⁵ Although it is clear that the present calculations are qualitatively consistent with the laboratory data, it is important that the discrepancy between the $v=1$ ^{13,14} and the $v=2,3$ ¹⁵ measurements be resolved because of the impact on the modeling of NO emission in the thermosphere.

It is clear from the present QCT calculation that the vibrational relaxation on both the ^2AB and ^2AC potential energy surfaces occurs exclusively through the formation of the NO₂ complex. Therefore, it is interesting to compare the present results with the statistical adiabatic channel model of Quack and Troe¹⁷ which was developed for unimolecular dissociation. Their approach uses known molecular properties and high pressure recombination rate constants of NO₂ to calculate the temperature dependence of NO(v) relaxation by O atoms. At 300 K, their model predicts relaxation rate constants of 1.7×10^{-11} cm³/s and 2.0×10^{-11} cm³/s for NO $v=1$ and $v=2$, respectively. These values are approximately 50% lower than the QCT relaxation rate constants of 2.8×10^{-11} cm³/s and 3.1×10^{-11} cm³/s for NO $v=1$ and $v=2$.

However, Quack and Troe assumed that only the ground state $^2\text{ABPES}$ participates in the relaxation process. Based on the recent work of Katagiri and Kato, the $^2\text{AC PES}$ should also be considered in calculation of the relaxation rate constant which would increase the Quack and Troe result by up to a factor of 2. For the QCT calculation, the $^2\text{AC PES}$ contributes approximately 25% to the relaxation rate constant, which indicates the present results for $\text{NO}(v=1,2)$ are in excellent agreement with the statistical model of Quack and Troe for the ground state surface.

Figure 4 shows the calculated temperature dependence of the $v=1$ to $v_B=0$ relaxation rate coefficient compared to the experimental measurements. As discussed previously, the calculated room temperature results are up to a factor of ~ 2 too low compared to experiment. However, the comparison of the high temperature results with the measurements of Glanzer and Troe¹⁶ are in excellent agreement. Although the temperature dependence of the QCT relaxation rate constant shows less than a 5% variation over the temperature range of 300 K to 2700 K, the rate constant calculated without including the electronic degeneracy factor actually increases by a factor of 1.65. The effect of including the temperature dependence of the electronic degeneracy factor for the $^2\text{ABand } ^2\text{AC}$ surfaces defined in Equation (10), which decreases from 0.095 at 300 K to 0.060 at 2700 K, is to produce a rate constant which is independent of temperature. As temperature increases, more collisions occur on the higher lying repulsive potential energy surfaces which are ineffective in vibrational relaxation. Thus, it is important to distinguish between the temperature-dependent effects due to the population of electronic states and the vibrational relaxation on the particular PES. Clearly, for systems as complicated as $\text{O}+\text{NO}$, establishing a mechanism (i.e., statistical behavior) for vibrational relaxation can not be decided by the overall temperature dependence of the rate constant alone. It is interesting to note that the relaxation rate constant predicted by the statistical adiabatic channel model¹⁷ decreases from $1.7 \times 10^{-11} \text{ cm}^3/\text{s}$

at 300 K to 1.2×10^{-11} cm³/s at 2100 K in disagreement with the QCT temperature independent relaxation rate indicating that the present calculations do indeed have a significant nonstatistical component.

There is currently only limited experimental²⁴ and theoretical information¹⁷ concerning the importance of multiquantum versus single quantum relaxation for O+NO(v). The *ab initio* electronic structure calculations,²³ which indicate that the NO vibrational relaxation occur on surfaces dominated by a strongly bound complex, would argue for efficient multiquantum relaxation.^{17,32} In fact, it has been shown by Glanzer and Troe for NO(v=2) at high temperatures (2700 K) and Fernando and Smith for NO(v=1) at room temperature that the vibrational deactivation is consistent with the formation of a collision complex. In addition, the recent measurements of Dodd et al.²⁴ for v=3 to vB=2 relaxation rate coefficient confirms the expectation of multiquantum relaxation. However, no information on the relaxation of highly vibrationally excited NO currently exists. Detailed QCT calculations of the vibrational relaxation of NO(v' 9) by oxygen atoms at 300 K are shown in Figure 5. The results, which indicate that multiquantum relaxation is very efficient, are independent of final state and can be qualitatively represented by $k_{vv'} = k_v / v$. Furthermore, the present results are in qualitative agreement with the results of the statistical adiabatic channel model¹⁷ for NO(v=1,2) and the expectations of statistical theories^{17,33,34} which predict that vB=0 should be the most populated final vibrational state independent of initial v. Finally, the experimental branching fraction of 0.35~0.10 for v=3 to vB=2 measured by Dodd et al. is in excellent agreement with the QCT calculated value of 0.29~0.02 providing further evidence of efficient multiquantum relaxation in O+NO collisions.

It is difficult to establish whether a particular dynamical system can be described by statistical theories. Wagner and Parks³⁴ have discussed in detail a general framework encompassing classical statistical theories, with emphasis on the

concept of a strong coupling region. This approach was employed in previous work³³ investigating the dynamical origin of statistical behavior in classical systems which exploited the sensitivity of classical dynamics to initial conditions. It was argued that exponential divergence of trajectories initially adjacent in phase space was responsible for memory loss in bimolecular collisions. Since such a detailed study is beyond the scope of the present work, one can use simple criterion for statistical behavior in the O+NO relaxation, for example, the ratio of the reactive (i.e., O atom exchange) to nonreactive relaxation rate constant. In a symmetric system, such as O+NO where the reactants and products are identical, any statistical theory would predict the ratio of the nonreactive to reactive relaxation rate constant to be unity.³³ This expectation implicitly assumes that the potential energy surface is symmetric with respect to the interchange of reactants and products. The simple test of this hypothesis for the O+NO(v) relaxation is illustrated in Figure 6, where the reactive and nonreactive components of the vibrational relaxation rate constants presented in Figure 3 are shown. The QCT results indicate that the nonreactive relaxation process is approximately a factor of 2 more efficient than the reactive O atom exchange relaxation for all initial vibrational states. This result implies that although the NO(v) relaxation proceeds via a collision complex and vibrational energy may or may not be equilibrated, the large fraction of the collisions which favor reforming reactants indicates significant *nonstatistical* behavior. Similar results have been observed in a molecular beam study³⁵ of the reactions of alkali atoms with alkali halides and in a QCT study³⁴ of alkali halide exchange reactions. Thus, the extent of statistical behavior in O+NO(v) relaxation remains to be firmly established.

5. Summary

Detailed quasiclassical trajectory calculations of the O+NO(v) vibrational relaxation rate constants have been carried out using the two lowest electronic

potential energy surfaces neglecting nonadiabatic interactions. The calculated total relaxation rate constants are in good agreement with the available experimental data and the statistical adiabatic channel model of Quack and Troe. Furthermore, the QCT calculations of the state-to-state relaxation rate constant show the importance of multiquantum vibrational energy transfer, again consistent with statistical behavior, and in excellent agreement with the recent experimental measurement of the $v=3$ to $v_B=2$ branching ratio by Dodd et al. Although the relaxation is shown to proceed exclusively through the formation of a long-lived bound intermediate, and the state-to-state rate constants are in good agreement with expectations based upon statistical theories, the branching ratio (i.e., nonreactive vs. O atom exchange) indicates that the collision complex retains some memory of the initial state.

The present results and the recent measurements of Dodd et al. for $\text{NO}(v=2,3)$ imply that the $\text{O}+\text{NO}(v=1)$ relaxation rate constant may be a factor of 2-3 smaller than previously thought. Reducing the $\text{NO}(v=1)$ relaxation rate constant used in NO thermospheric cooling rate calculations would require higher atmospheric temperatures and/or an increase in the NO/O number densities in the models to maintain agreement with measurements. The suggestion of higher thermospheric NO densities for cooling rate calculations is consistent with numerous measurements of NO densities in the lower thermosphere which show that measured values are generally larger than those predicted by photochemical models.

Acknowledgments. This research has been supported by AFOSR under task 2303 EP and Phillips Laboratory project 007.

References

- 1 G. Kockarts, *Geophys. Res. Lett.*, 1980, **7**, 137.
- 2 A. S. Zachor, R. D. Sharma, R. M. Nadile, and A. T. Stair, *J. Geophys. Res.*, 1985, **90**, 9776.
- 3 J. P. Kennealy, F. P. Del Greco, G. E. Caledonia, and B. D. Green, *J. Chem. Phys.*, 1978, **69**, 1574.
- 4 B. D. Green, G. E. Caledonia, W. A. M. Blumberg, and F. H. Cook, *J. Chem. Phys.*, 1984, **80**, 773.
- 5 W. T. Rawlins, M. E. Fraser, and S. M. Miller, *J. Phys. Chem.*, 1989, **93**, 1097.
- 6 J. W. Duff, F. Bien, and D. E. Paulsen, *Geophys. Res. Lett.*, 1994, **21**, 2043.
- 7 R. D. Sharma, Y. Sun, and A. Dalgarno, *Geophys. Res. Lett.*, 1993, **20**, 2043.
- 8 R. D. Sharma, H. Dothe, F. von Esse, V. A. Kharchenko, Y. Sun, and A. Dalgarno, *J. Geophys. Res.*, 1996, **101**, 19,707.
- 9 B. Hubert, J.-C. Gérard, V. I. Shematovich, D. V. Bisikalo, *Geophys. Res. Lett.*, 1996, **23**, 2215.
- 10 J. O. Wise, R. L. Carovillano, H. C. Carlson, R. G. Roble, S. Adler-Golden, R. M. Nadile, and M. Ahmadjian, *J. Geophys. Res.*, 1995, **100**, 21,357.
- 11 D. Bose and G. V. Candler, *J. Chem. Phys.*, 1996, **104**, 2825.
- 12 J.-C. Gérard, V. I. Shematovich, D. V. Bisikalo, *Geophys. Res. Lett.*, 1995, **3**, 279.
- 13 R. P. Fernando and I. W. M. Smith, *Chem. Phys. Lett.*, 1979, **66**, 218.
- 14 H. V. Lilenfeld, *PL-TR-94-2180*, 1994, Phillips Laboratory Final Rep.
- 15 J. A. Dodd, S. M. Singleton, S. M. Miller, P. S. Armstrong, and W. A. M. Blumberg, *Chem. Phys. Lett.*, 1996, **260**, 103.
- 16 K. Glanzer and J. Troe, *J. Chem. Phys.*, 1975, **63**, 4352.

- 17 M. Quack and J. Troe, *Ber. Bunsenges. Physik. Chem.*, 1975, **79**, 170.
- 18 G. D. Gillispie, A. U. Khan, A. C. Wahl, R. P. Hosteny, and M. Krauss, *J. Chem. Phys.*, 1975, **63**, 3425.
- 19 C. F. Jackels and E. R. Davidson, *J. Chem. Phys.*, 1975, **63**, 4672; *ibid.*, 1976, **64**, 2908.
- 20 G. Hirsh and R. J. Buenker, *Can. J. Chem.*, 1985, **63**, 1542.
- 21 G. Hirsh, R. J. Buenker, and C. Petrongolo, *Mol. Phys.*, 1990, **70**, 835; *ibid.*, 1991, **73**, 1085.
- 22 C. P. Blahous, B. F. Yates, Y. Xie, and H. F. Schaefer, *J. Chem. Phys.*, 1990, **93**, 8105.
- 23 H. Katagiri and S. Kato, *J. Chem. Phys.*, 1993, **99**, 8805.
- 24 J. A. Dodd, R. B. Lockwood, S. M. Miller, and W. A. M. Blumberg, *J. Chem. Soc., Faraday Trans.*, submitted for publication.
- 25 M. Gilibert, A. Aguilar, M. González, and R. Sayós, *Chem. Phys.*, 1993, **172**, 99.
- 26 G. Suzzi Valli, R. Orru, E. Clementi, A. Laganà, and S. Crocchianti, *J. Chem. Phys.*, 1995, **102**, 2825.
- 27 C. A. Parr and D. G. Truhlar, *J. Phys. Chem.*, 1971, **75**, 1844.
- 28 J. N. Murrell and K. S. Sorbie, *J. Chem. Soc., Faraday Trans.*, 1974, **70**, 1552.
- 29 D. G. Truhlar and J. T. Muckerman, in *Atom-Molecule Collision Theory*, ed. R. B. Bernstein, Plenum, New York, 1979, p. 505.
- 30 M. M. Graff and A. F. Wagner, *J. Chem. Phys.*, 1990, **92**, 2423.
- 31 P. Brumer, *J. Comp. Phys.*, 1974, **14**, 391.
- 32 P. Brumer and M. Karplus, *Disc. Faraday Soc.*, 1973, **55**, 80.

- 33 J. W. Duff and P. Brumer, *J. Chem. Phys.*, 1977, **67**, 4898; *ibid.*, 1979, **71**, 2693.
- 34 A. F. Wagner and E. K. Parks, *J. Chem. Phys.*, 1976, **65**, 4343.
- 35 W. B. Miller, S. A. Safron, and D. R. Herschbach, *Disc. Faraday Soc.*, 1967, **44**, 108.

TABLE 1. Parameters for the LEPS Potential^a

	D_e	r_e	a_1	a_2	a_3	z
NO($X^2\Pi_{1/2}$)	6.6144	1.1508	5.035	5.151	2.998	0.3
O ₂ ($X^3\Sigma + g$)	5.2132	1.2075	5.476	7.950	6.341	0.2

^aThe diatomic parameters are taken from ref. 25. Energies are given in eV and distances in Ångstroms.

TABLE 2. Parameters for the NO₂ 1²ABand 1²AC Exponential Functions^a

	1 ² AB	1 ² AC
c_0	19.00085	48.52510
c_1	-62.34160	-194.92802
c_2	52.40209	245.46673
c_3	-9.43063	-93.79654
γ	2.30	2.30
r^o	1.195	1.270

^aEnergies are given in eV and distances in Ångstroms.

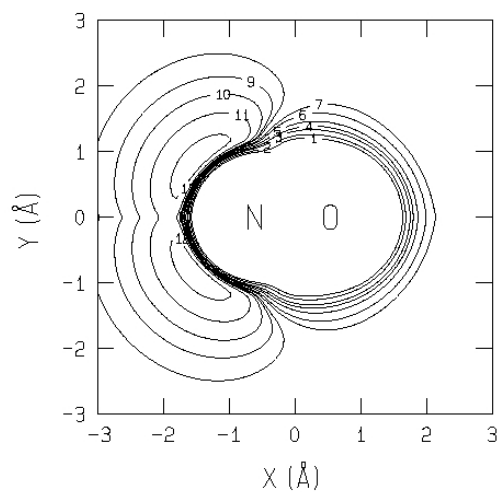


Figure 1. Polar contour plot of the $\text{ONO } ^2\text{AB}$ potential energy surface with the NO internuclear distance set equal to its equilibrium value. The contour values in eV are 4(1), 3(2), 2(3), 1.5(4), 1(5), 0.5(6), 0.25(7), -0.1(8), -0.25(9), -0.5(10), -1(11), and -2(12) relative to the $\text{O}(^3\text{P})+\text{NO}(^2\Pi_{1/2})$ asymptote.

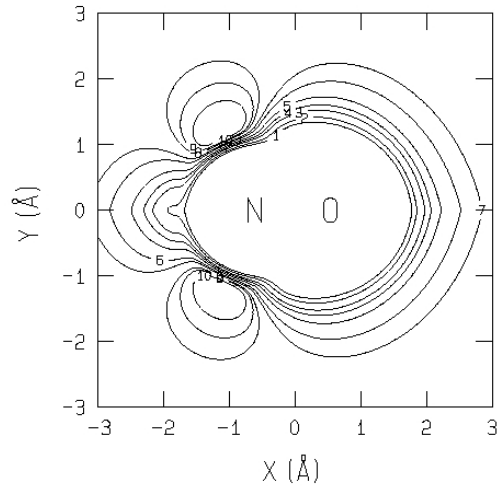


Figure 2. Polar contour plot of the $\text{ONO } ^2\text{AC}$ potential energy surface with the NO internuclear distance set equal to its equilibrium value. The contour values in eV are 4(1), 3(2), 2(3), 1.5(4), 1(5), 0.5(6), 0.25(7), -0.1(8), -0.25(9), and -0.5(10) relative to the $\text{O}(^3\text{P})+\text{NO}(^2\Pi_{1/2})$ asymptote.

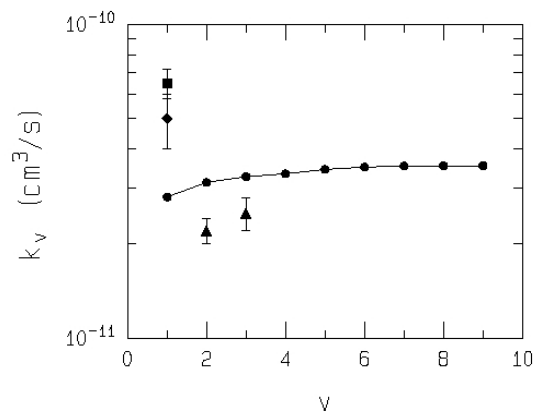


Figure 3. Room temperature (300 K) rate coefficient for the deactivation of vibrationally excited $\text{NO}(v)$ upon impacts with atomic oxygen as function of the vibrational level. The present QCT(nMn) calculation is compared to the experimental measurements of Fernando and Smith¹³ (#), Lilenfeld¹⁴ (u), and Dodd et al.¹⁵ (2). The rate coefficient k_v is the sum of the rate coefficients for deactivation to all the final levels, $k_v = \sum_{v' \neq v} k_{vv'}$.

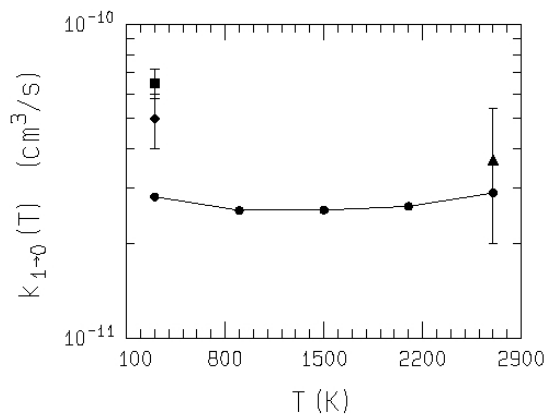


Figure 4. Temperature dependence of the vibrational deactivation of $\text{NO}(v=1)$ by atomic oxygen. The present QCT(nMn) calculation is compared to the experimental measurements of Fernando and Smith¹³ (#), Lilenfeld¹⁴ (u), and Glanzer and Troe¹⁶ (2).

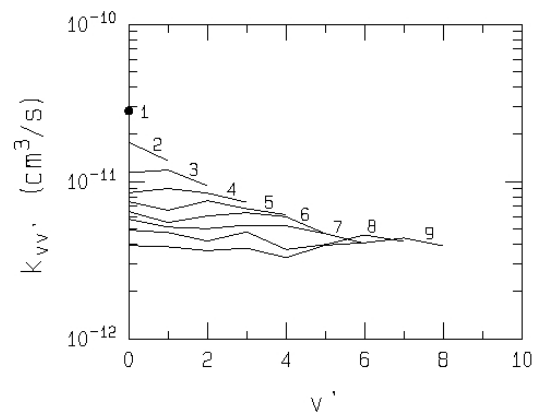


Figure 5. Rate coefficients for the deactivation of $\text{NO}(v)$ to $\text{NO}(v')$ by atomic O as a function of the final vibrational level v' . The final vibrational levels are connected by solid lines for clarity of presentation and the initial level v is indicated on each curve.

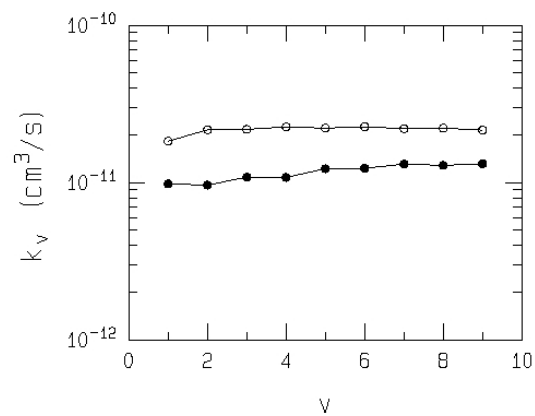


Figure 6. The contribution of the nonreactive ($n \rightarrow n$) and O atom exchange ($n \rightarrow n$) reactions to the rate coefficient for vibrational relaxation k_v at room temperature as a function of the initial vibrational level v .